Progress In Electromagnetics Research M, Vol. 9, 41–52, 2009

SCATTERING AND IMAGE SIMULATION FOR RECONSTRUCTION OF 3D PEC OBJECTS CONCEALED IN A CLOSED DIELECTRIC BOX

J. Dai and Y.-Q. Jin

Key Laboratory of Wave Scattering and Remote Sensing Information (MoE)
Fudan University
Shanghai 200433, China

Abstract—A new approach of imaging reconstruction of concealed PEC targets in a dielectric closed box, using azimuth multi-angle measurements, is developed. As the broadband stepped-frequency radar transmits planar wave from different azimuth directions around the target, the backscattered electrical fields in both the amplitude and phase are obtained. The two-dimensional fast Fourier transform (2D-FFT) algorithm for spline interpolation is adopted for uniformly sampled backscattering fields. Then, 2D difference image from a dielectric box with and without the concealed targets can be numerically simulated. Multi-azimuth backscattering electrical fields of complex shaped PEC (Perfect Electric Conductor) targets and dielectric surrounding walls are calculated by the method of moments (MoM), which is based on the coupled volume-surface integral equation (VSIE). The concealed targets can be well identified from the imaging reconstruction.

1. INTRODUCTION

Detection and localization of the concealed targets in unaccessible environment have been of interest in both military and civilian applications [1–11], such as the surveillance and detection of the target concealed in the closed surrounding walls, which is visually opaque, the early-warning for possible dangers, e.g., bomb and grenade, and the rescue mission for searching survivors in earthquake or avalanche, etc. A key issue is how to quickly identify the target from the blurred image caused by complicated interactions between the object and surrounding

Corresponding author: Y.-Q. Jin (yqjin@fudan.ac.cn).

obstacle in real-time situation, especially for surveillance and early-warning.

Some techniques of detection and imaging for the target behind a wall have been developed in [3–10], such as synthetic aperture beamformer and Capon beamformer using multiple stationary antennas. However, it has been known that these beamformer methods were usually very time-consuming due to low computational efficiency. A high-frequency asymptotic ray-tracing technique was also applied to analysis of scattering interactions in a building and reconstruction of building interior image by implementing conventional FFT [11]. The sheltering effects of the wall may blur the image and shift the target position, as first discussed in computer simulation. A refocusing approach was applied to removal of the wall effect [9]. Usually, it was necessary to first evaluate the wall parameters, i.e., wall thickness, dielectric property etc., using the optimization method for compensation of the perturbation caused by the wall using the method of match filtering. However, this evaluation might not be accurate enough, especially for inhomogeneous walls.

In this paper, a closed 3D dielectric box to enclose the targets, e.g., multi-spheres, pistol etc., is modeled. The imaging approach with FFT is applied to significantly improve the computational efficiency. A two-dimensional (2D) difference image from a dielectric box with and without the targets is numerically simulated and well eliminates the complicated sheltering of the box and interaction with the targets without prior evaluation of the wall parameters.

An image reconstruction of concealed targets in a closed box, using stepped frequency, is described. As the broadband stepped-frequency radar transmits planar wave from different azimuthal directions around the target, the backscattered electrical fields in both the amplitude and phase are recorded. Comparing with the case without the targets, which has been assumed as known, the difference image can eliminate the interaction and show the existence of the targets. The backscattering electrical fields of complex shaped conducting and dielectric targets are calculated by conventional method of moments (MoM), which is based on the coupled volume-surface integral equation.

To improve high computational efficiency, 2D-FFT is employed to the uniformly sampled scattering fields. The 2D spline interpolation makes good tradeoff between the efficiency and accuracy of the calculation. Then, the 2D image is reconstructed to identify the targets existence. This technique is applicable to detection and localization of the PEC targets, e.g., concealed inside unaccessible box. It is convenient to obtain high-resolution, high-quality and real-time image.

2. THE PRINCIPLE OF IMAGING BASED ON POINT SCATTERING

The volumetric target is numerically divided into finite point units for numerical calculation of scattering fields. Making the radar source and receiver locate in the cross-sectional plane, as shown in Fig. 1, the radar wave is incident upon these point units to yield azimuthal scattering measurements of the 3D object in both the amplitude and phase.

The distance between the receiver A and scattering point (x, y), which is an arbitrary point unit of the object, can be written as

$$\begin{aligned} R &= \sqrt{(R_0\cos\theta - x)^2 + (R_0\sin\theta - y)^2} \\ &= \sqrt{R_0^2 - 2R_0(y\sin\theta + x\cos\theta) + (x^2+y^2)} \end{aligned} \tag{1}$$

where θ is the incident angle.

The received scattering signal at the location A is

$$V(f,\theta) = \delta\exp(-j4\pi R/\lambda) \tag{2}$$

where δ is the reflection coefficient of the scattering point; λ is the incident wavelength.

Total scattering electrical field $G(f,\theta)$ received by the radar at location A can be regard as the integral of all of the point units shown as following,

$$G(f,\theta) = \iint g(x,y)\exp(-j4\pi R/\lambda)dxdy \tag{3}$$

The radar echo at each location A along the circle orbit (indicated by the dashed line in Fig. 1), $G(f,\theta)$, is numerically calculated by the

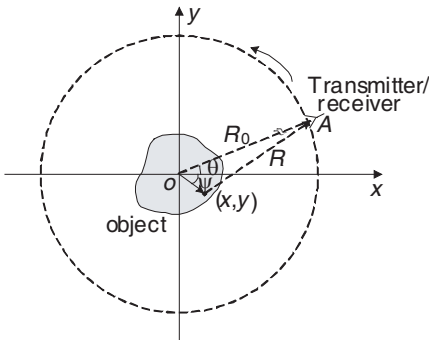

Figure 1. Imaging geometry of a 3D object in x-y plane.

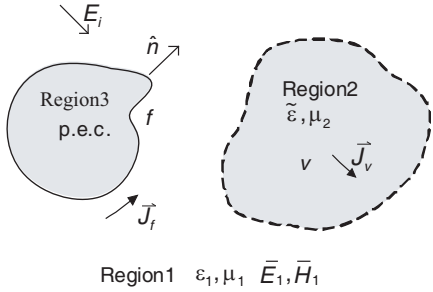

Figure 2. Mixed scattering object model composed of conductor and dielectric.

method of moment (MoM) of commercial software package FEKO. From the imaging theory, it has been known [12] that the scattering field $G(f,\theta)$ is the Fourier transformation of the reflectivity density function, $g(x,y)$, in the x-y plane.

Using 2D delay-and-sum (DS) spatial beams [8], the inverse Fourier transform is applied to Eq. (3) in a summation form, and yields

$$g(x,y) = \frac{1}{N_g N_h} \sum_{g=0}^{N_g-1} \sum_{h=0}^{N_h-1} w(f_g,\theta_h) G(f_g,\theta_h) \exp(j4\pi R_h/\lambda_g) \qquad (4)$$

where N_g is the number of the frequencies of the incident wave; N_h is the number of the locations. R_h is the range between the h-th antenna and scattering point, and $w(f_g,\theta_h)$ is an optional window function which is used to reduce the effect of the sidelobe.

Equation (4) produces a 2D reconstruction image, which was usually studied by using the backprojection method (BP) [13]. However, due to low efficiency of BP with complexity $o(M^2 m)$, it seems very difficult to fulfill the algorithm of imaging the electric large targets. Here M is the pixel number of the image, and $m = N_h(1+E)(N_g+3)$ is the computational complexity to get one image pixel where E is the computational complexity for multiplication [8]. The FFT algorithm is employed for reconstruction of the 2-D image.

Now, consider a mixed scattering object composed of conductor and dielectric as shown in Fig. 2. When a plane wave $\vec{E}_i$ is incident upon the hybrid object, it produces the scattering field $\vec{E}_s$ (indicated by the subscript s), which can be written as [13]

$$\vec{E}_s(\vec{r}) = -j\omega\vec{A}_f(\vec{r}) - \nabla\Phi_f(\vec{r}) - j\omega\vec{A}_v(\vec{r}) - \nabla\Phi_v(\vec{r}) \qquad (5)$$

where $\vec{A}_f(\vec{r}), \Phi_f(\vec{r})$ are, respectively, the magnetic vector and electric scalar generated by the surface current J_f, and $\vec{A}_v(\vec{r}), \Phi_v(\vec{r})$ are, respectively, the magnetic vector and electric scalar generated by the body current J_v.

The boundary conditions on the metal surface and in the body medium are written as:

$$\begin{cases} \vec{E}(\vec{r}) = \vec{E}_i(\vec{r}) + \vec{E}_s(\vec{r}) & \vec{r} \in v \\ \vec{n} \times [\vec{E}_i(\vec{r}) + \vec{E}_s(\vec{r})] = 0 & \vec{r} \in f \end{cases} \qquad (6)$$

The metal surface current J_f can be expanded based on the RWG vector basis functions in triangular [14]. And the electric field $\vec{E}(\vec{r})$ in the body medium can be expanded through the tetrahedral mesh and the corresponding SWG basis functions, as discussed in [15].

Substituting Eq. (5) into Eq. (6), using Garlerkin's matching method, one can obtain independent equations with $N_f + N_v$ unknowns in the matrices as follows,

$$\begin{bmatrix} Z_{ff} & Z_{fv} \\ Z_{vf} & Z_{vv} \end{bmatrix} \begin{bmatrix} I_{fn} \\ I_{vn} \end{bmatrix} = \begin{bmatrix} E_f \\ E_v \end{bmatrix} \tag{7}$$

where E_f, E_v are the scattering fields produced by the surface and body volume, respectively, and all other terms can be found in 14]. Using commercial software FEKO to solve Eq. (7), the total scattered electrical fields $\vec{E}_s(\vec{r})$, i.e., E_f+E_v, can be obtained, and denote $G(f,\theta)$ as its horizontally polarized component for our imaging simulation and reconstruction.

3. THE IMAGING ALGORITHM OF 2D FFT

Due to far field $R_0 \gg x, y$, it makes $R \approx R_0 - (y\sin\theta + x\cos\theta)$. The scattered electrical field received at location A, which has been numerically calculated, is written as:

$$G(f,\theta) = \iint g(x,y)\exp[j4\pi/\lambda(x\cos\theta + y\sin\theta)]dxdy \tag{8}$$

where the constant coefficient $\exp(-j4\pi R_0/\lambda)$ is simply ignored. Substituting

$$\begin{cases} X = 2\cos\theta/\lambda = 2f\cos\theta/c \\ Y = -2\sin\theta/\lambda = 2f\sin\theta/c \end{cases} \tag{9}$$

into Eq. (8), it yields

$$G(X,Y) = \iint g(x,y)\exp[j2\pi(xX + yY)]dxdy \tag{10}$$

It is seen that $G(X,Y)$ of Eq. (16) is the 2D inverse Fourier transform of $g(x,y)$, and 2D Fourier transform yields

$$g(x,y) = \int_{-\infty}^{+\infty}\int_{-\infty}^{+\infty} G(X,Y)\exp[-j2\pi(xX + yY)]dXdY \tag{11}$$

To take advantage of 2D-FFT, interpolation is employed to make the data sampling uniformly in spatial spectrum domain, as follows,

(1) The bandwidth of the incident wave makes m-stepped frequencies uniformly within $(f_1 - f_2)$. Backscattering fields $G(f_m, \theta_n)$ for different incident angle θ_n and each frequency f_m are measured.

(2) Determine the sampling region and density. To make full use of the measured data and uniformly sample in FFT, a rectangle region is chosen as shown in Fig. 3(a), which is close to the annulus region of measured data. The sample density is similar to the measured data. The region is equally divided in X and Y directions, indicated by (i, j). It describes the grid coordinate as

$$X_i = X_1 + (i-1)\Delta X, \quad Y_j = Y_1 + (j-1)\Delta Y$$

(3) The relation between f, θ and X, Y is:

$$f = c\sqrt{X^2 + Y^2}/2, \quad \theta = \tan^{-1}(Y/X) \tag{12}$$

Mapping (X_i, Y_j) onto (f_i, θ_j), the resample points A and C in Fig. 3 are not located in the measured region and set $G(f_i, \theta_j) = 0$. The electrical field of B' mapped from B might be unknown as no recorded. It is feasible to get them by interpolation on f-θ plane from the measured data. To get the balance between computational efficiency and accuracy, 2D cubic spline interpolation is employed. Eq. (4) shows that the data truncation imposes a rectangle window to the sample data, which raises sidelobe. To reduce the sidelobe effect, the resample data is weighted by a tapered cosine window before interpolation.

(4) Apply 2D FFT to the uniformly resampled data on the X-Y plane to yield 2D reconstruction image $g(x, y)$.

4. SIMULATION RESULTS

In the stepped-frequency system, the echo signals are contributed by backscattering and interaction of the targets and box walls. We take the measures to eliminate the aforementioned effects as follows,

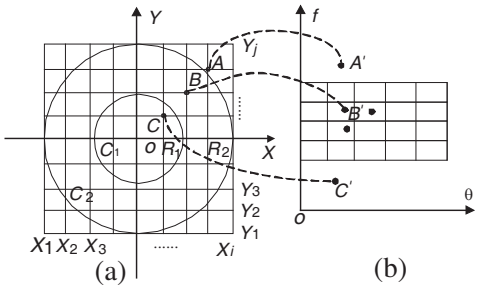

Figure 3. Sample mapping from X-Y plane to f-θ plane.

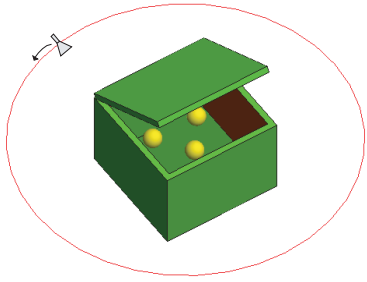

Figure 4. Three PEC spheres concealed in a dielectric box.

(1) The scattering from the box without the targets are first calculated, which can be seen as a priori condition. The backscattering fields are obtained (calculated) as G_b.

(2) Measure the backscattering electrical field of real scene that the target is concealed in a dielectric closed box. The scattering from the box with concealed targets is calculated, as G_r.

(3) The difference of these two cases, i.e., $G_r - G_b$, might be able to show the target existence using the approach mentioned above.

Numerical simulation of scattering fields $G(f, \theta)$ is performed using commercial software FEKO which is based on the MOM of the coupled volume-surface integral equation (VSIE), performed on the parallel computers Dell Poweredge. As an example, two cases of the objects of three PEC spheres (Fig. 4) and a PEC pistol (Fig. 9) are concealed in a dielectric rectangular box.

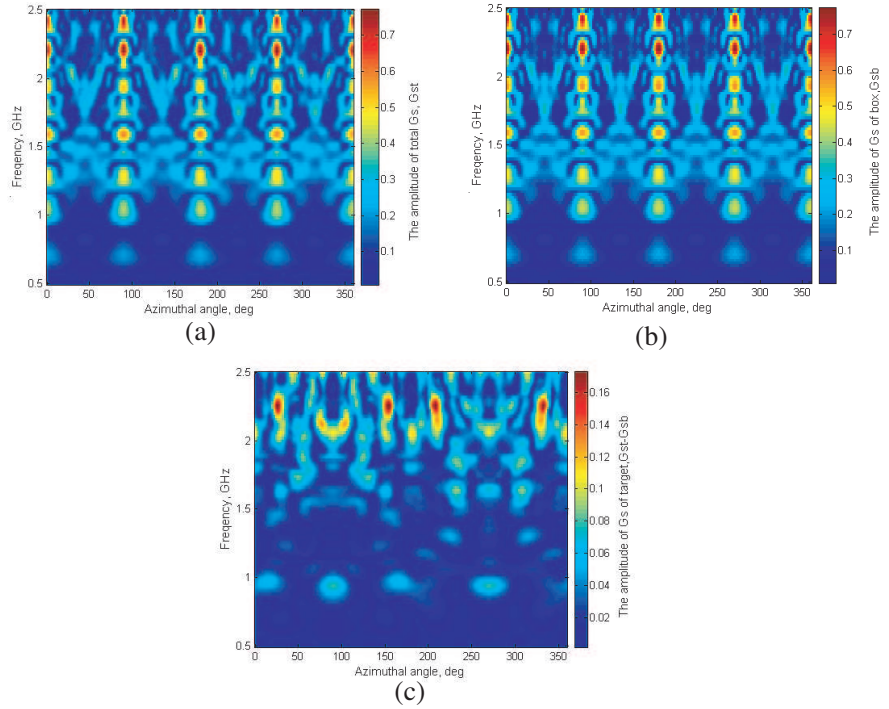

Figure 5. The amplitude of the difference backscattered fields. (a) Total scattered field from the box with targets. (b) Scattering field from the box without targets. (c) Difference scattering field of (a) and (b).

Case I: The closed dielectric box is 0.4 m long, 0.4 m wide and 0.3 m high. The wall thickness of the box is 2 cm, and its dielectric constant is 4.0. Three PEC spheres with the same radius 0.03 m are concealed in $S_1(0.0, 0.08)$ m, $S_2(-0.08, -0.08)$ m, $S_3(0.08, -0.08)$ m inside the box. In MoM calculation, the geometric surfaces of the three spheres and body of the dielectric are meshed into 954 triangles and 21341 tetrahedrons.

The H-(horizontally) polarized planar wave is incident perpendicularly onto the box wall. The stepped-frequency signals between 0.5 GHz and 2.5 GHz with 20 MHz interval are transmitted from the radar around the box in every 2°. The parameters $N_g = 101$ and $N_h = 180$ are taken. The co-polarized (HH) backscattering electrical fields, G_{HH}, are obtained, as shown in Figs. 5(a)–(c).

Figure 5(a) is the total scattering fields of the targets (3 PEC spheres) and the box for incident angle vs the frequency; Fig. 5(b) is the scattering fields from the box without the targets; Fig. 5(c)

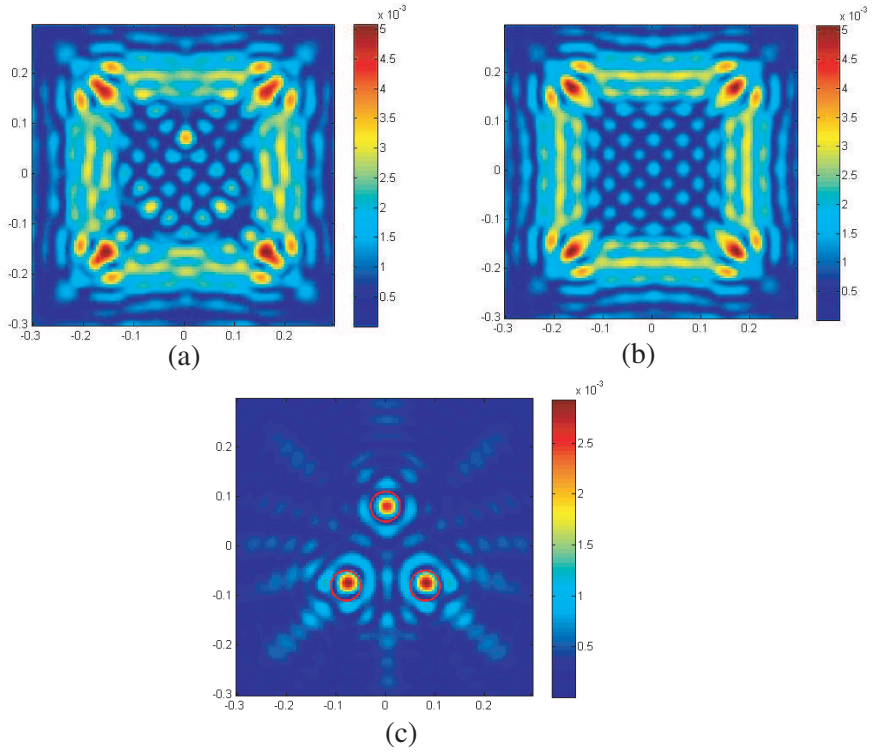

Figure 6. Image and detection. (a) Image of three spheres in a box. (b) Image of a box without targets. (c) Detection of three spheres.

is the difference fields of the cases with and without targets. This measurement (calculation) is repeated at 180° uniformly azimuth directions. It can be seen that strong periodic reflections come from the box walls at 0°, 90°, 180° and 270°, respectively.

Using the approach proposed above and $G(f, \theta)$ of Figs. 5(a)–(c), the image of $g(x, y)$ can be constructed. Figs. 6(a) and (b) present the image of the box with and without the targets, and Fig. 6(c) gives the detection of three PEC spheres from the images.

It can be seen that three sphere targets can be identified in Fig. 6(a), even the locations are a little deviated from correct positions. Fig. 6(c) gives final detection, and some false clutters are eliminated, where the red circles indicate the real locations of three spheres on the imaging plane.

In order to estimate the influence caused by the dielectric box walls, a complex dielectric constant of the box walls is assumed as $4.0 - j0.02$, and the other parameters are kept. From Fig. 7, we can see that dielectric loss makes radar echo signal weaker. However, the reconstruction image still has a clear profile, and its result is also good enough as shown in Fig. 8.

Case II: Another case is that a metallic pistol is concealed in a dielectric box, as shown in Fig. 9.

The box is 0.4 m long, 0.4 m wide and 0.3 m high. The wall thickness is 2 cm, and its dielectric constant is 4.0. The dimension of the metal pistol is 13 cm × 8.5 cm. In MoM calculation, the geometric surfaces of the three spheres and body of the dielectric are meshed into 2410 triangles and 79058 tetrahedrons.

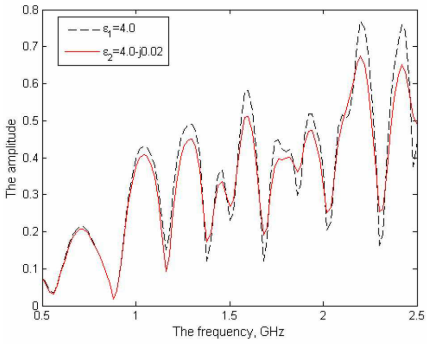

Figure 7. The amplitude of scattering fields of different frequencies for real and complex dielectric walls.

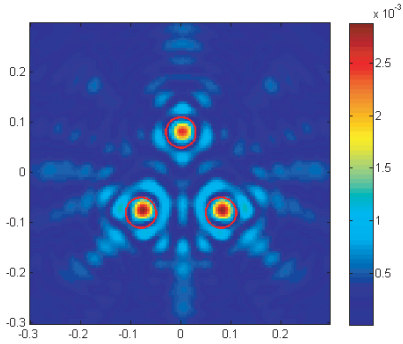

Figure 8. Reconstructed three balls in a loss box.

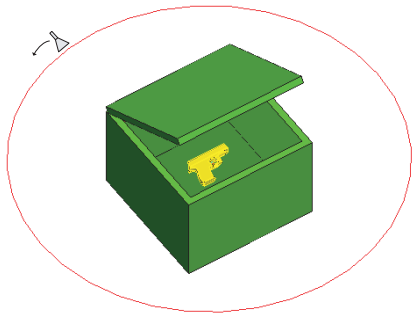

Figure 9. A metallic pistol concealed in a box.

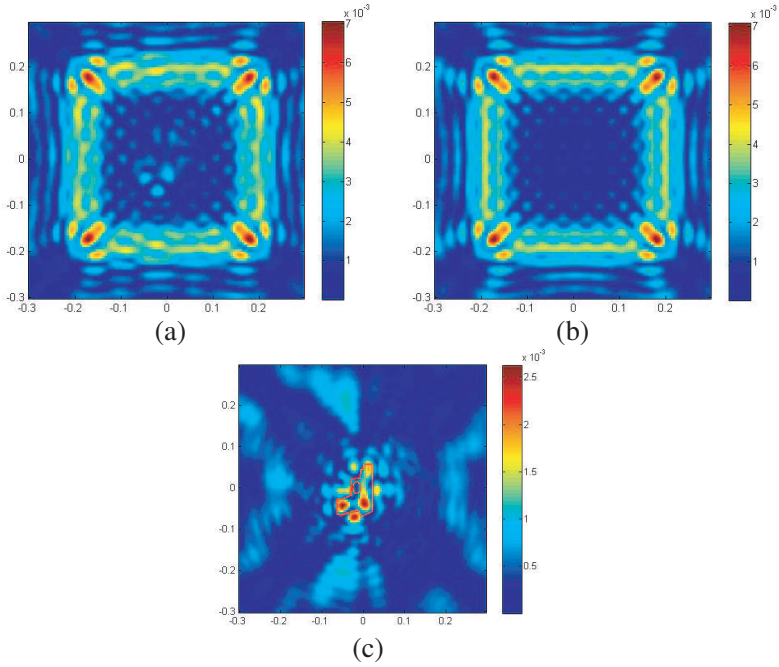

Figure 10. Reconstructed image of the pistol target. (a) The image with the pistol. (b) The image without the pistol. (c) The difference image for pistol detection.

The stepped-frequency signals between 0.5 GHz and 3.0 GHz with 20 MHz interval are vertically incident onto the box at every azimuth 2°. Total 180° backscattering fields are uniformly recorded. The bandwidth of the incident electromagnetic wave is increased for higher

resolution. The parameters $N_g = 126$ $N_h = 180$ are taken.

Figures 10(a) and (b) give the image with and without the pistol, respectively. The interference of the box with the pistol target can be visually identified. In Fig. 10(b), it can be seen that there are strong reflections, especially in the box corners, which might cause confusion for target detection. Fig. 10(c) is produced by the difference of the scattering fields with and without the targets. It can identify the existence of the target at correct positions. In Fig. 10(c), the pistol profile of the reconstruction image can be quickly identified and well matches to the real location (described by a red profile). Increasing the bandwidth can obtain higher resolution.

If the dielectric constant of the box is increased, e.g., to 4.0, it might enhance stronger interactions between the box wall and target, and cause more difficulty to detect the targets.

5. CONCLUSION

Numerical simulations of scattering and image show the feasibility for detection and location of the targets concealed in a dielectric box. High-resolution reconstruction image in real time can be obtained. It needs to collect echoes from some aspects around the target. At the same time, the high efficient calculation can produce the target image in real time to achieve the detection, surveillance, early-warning for the target. The physical properties of the surrounding box, e.g., thickness, dielectric constant and shape, etc. can affect the final quality of detection, even making the imaging results blurred. It can be further improved by increasing the bandwidth for high resolution, etc. These issues remain for future research.

ACKNOWLEDGMENT

This work was supported by the National Science Foundation of China 60971091 and 406370338.

REFERENCES

1. Ferris, Jr., D. D. and N. C. Currie, "Microwave and millimeter-wave systems for wall penetration," *Proc. SPIE*, Vol. 3375, 269–279, 1998.
2. Yang, Y. and A. E. Fathy, "See-through-wall imaging using ultra wideband short-pulse radar system," *Proc. IEEE Antennas Propag. Soc. Int. Symp.*, 334–337, 2005.

3. Wang, G., Y. Zhang, and M. Amin, "New approach for target locations in the presence of wall ambiguities," *IEEE Trans. Aerosp. Electron. Syst.*, Vol. 42, No. 1, 301–315, 2006.
4. Ahmad, F., M. G. Amin, and S. A. Kassam, "Synthetic aperture beamformer for imaging through a dielectric wall," *IEEE Trans. Aerosp. Electron. Syst.*, Vol. 41, No. 1, 271–283, 2005.
5. Wang, G. and M. Amin, "Imaging through unknown walls using different standoff distances," *IEEE Trans. Signal Process.*, Vol. 54, No. 10, 4015–4025, Oct. 2006.
6. Amin, M. G., "Radar, signal, and image processing techniques for through the wall imaging," *Proc. SPIE*, Vol. 5819, 33–45, 2005.
7. Ahmad, F., M. G. Amin, and S. A. Kassam, "A beamforming approach to stepped-frequency synthetic aperture through-the-wall radar imaging," *Proc. CAMSAP05*, Vol. 1, Dec. 2005.
8. Yoon, Y. S. and M. G. Amin, "High-resolution through-the-wall radar imaging using beamspace music," *IEEE Trans. on Antennas and Propag.*, Vol. 56, No. 6, 1763–1774, 2008.
9. Dehmollaian, M. and K. Sarabandi, "Refocusing through building walls using synthetic aperture radar," *IEEE Transactions on Geoscience and Remote Sensing*, Vol. 46, No. 6, 1589–1599, 2008.
10. Ferris, Jr., D. and N. Currie, "A survey of current technologies for through-the-wall surveillance (TWS)," *Proc. SPIE*, Vol. 3577, 62–72, 1998.
11. Chang, P. C., R. J. Burkholder, J. L. Volakis, R. J. Marhefka, and Y. Bayram, "High-frequency EM characterization of through-wall building imaging," *IEEE Transactions on Geoscience and Remote Sensing*, Vol. 47, No. 5, 1375–1387, May 2009.
12. Mensa, D. L., *High Resolution Radar Cross-section Imaging*, 139–151, Artech House, Norwood, MA, 1991.
13. Nie, X. C., N. Yuan, L. W. Li, et al., "A fast volume-surface integral equation solver for scattering from composite conducting-dielectric objects," *IEEE Trans. on Antennas and Propag.*, Vol. 53, No. 2, 818–824, 2005.
14. Rao, S. M., D. R. Wilton, and A. W. Glisson, "Electromagnetic scattering by surfaces of arbitrary shape," *IEEE Trans. on Antennas and Propag.*, Vol. 30, No. 3, 409–418, May 1982.
15. Schaubert, D. H., D. R. Wilton, and A. W. Glisson, "A tetrahedral modeling method for electromagnetic scattering by arbitrarily shaped inhomogeneous dielectric bodies," *IEEE Trans. on Antennas and Propag.*, Vol. 32, No. 1, 77–85, Jan. 1984.